

Radiographic imaging for the observation of Modes I and II fracture in Fibre Reinforced Concrete

S.J. Foster, G.G. Lee & T.N.S. Htut

School of Civil and Environmental Engineering, The University of New South Wales, Sydney, Australia

ABSTRACT: In this study, radiographic imaging is used to investigate the mechanisms of fracture in fibre reinforced concrete. The investigation looks at the performance of discrete end-hooked and straight fibres crossing a cracking plane at various angles and loaded normal or parallel to the plane. A main finding of the study is that in Mode II fracture, snubbing of fibres in the concrete adjacent to the crack interface provides significant mechanical anchorage. However, the strength benefits of this anchorage come only after significant slip displacement. Further, for acute angled fibres, due to the high anchorage provided by the snubbing, fibre fracture often governs over fibre pullout suggesting an increased brittle response compared to that of fibres subjected to crack opening (Mode I) fracture. Lastly, the tests clearly show that a significant proportion of fibres in Mode II failure pullout from the longer embedded side.

1 INTRODUCTION

Since Romualdi and Batson (1963) first performed tests on modern day fibre reinforced concrete (FRC), a significant body of research has been undertaken and reported in the literature. Studies such as those by Peterson (1980) have been undertaken on fibre reinforced mortar, with various percentages of fibres in the matrix, providing data on the tensile stress versus crack opening displacement (COD) response. Other studies, such as for example Banthia and Trotter (1994), have concentrated on the anchorage and pullout mechanisms of individual fibres crossing a join in a tensile specimen. Space in this paper prohibits an extensive review of the literature on tensile fracture of fibre reinforced cementitious composites. For a more comprehensive review we refer the reader to Voo and Foster (2003).

While a significant body of research has been undertaken on Mode I (crack opening) fracture of FRC over a period of 40 years and more, less research has been undertaken on Mode II fracture (also referred to as crack sliding). The first study on direct shear specimens was by Van de Loock (1987). In the time since studies have been conducted by Valle and Büyüköztürk (1993), Balaguru and Dipsia (1993), Khaloo and Kim (1997) and Mirsayah and Banthia (2002). However, these studies were generally limited and have not lead to a general understanding of the behaviour of fibre reinforced concrete subjected to longitudinal shear. A review of each of these test

series, highlighting strengths and weaknesses, is given in Lee and Foster (2006a).

Lee and Foster (2006a, 2006b) reported results of 39 discrete fibre test specimens in direct shear (Mode II), in addition to a series of fibre volume tests for straight and end-hooked fibres. The conclusions drawn from the studies were: (i) the load versus crack sliding behaviour is dependent on the fibre orientation across the shear plane; (ii) the critical length of a fibre for fibre fracture is significantly influenced by the angle that the fibre crosses the cracking plane; (iii) the combined effect of bending and axial force has a more pronounced effect on the fracture of acute angle fibres; (iv) due to the snubbing effect for the acute angle fibres, considerable displacement occurs before fibres become effectively engaged; (v) secondary anchor effects due to snubbing increase the load and displacement capacity; (vi) the common modelling assumption of pullout always from the shorter of side of fibre embedment is questioned and its influence requires further investigation; and (vii) the common assumption of uniform bond stress along the length of embedment is questioned and requires more study. In this study radiographic imaging is used to answer some of the questions posed by Foster and Lee (2006b) and to explore fundamental differences in behaviour between Mode I fracture and Mode II fracture of FRC.

2 EXPERIMENTAL PROGRAMME

2.1 Introduction

In this section, details of the uniaxial tension (UT) tests and direct shear (DS) tests are described. For the UT (Mode I) tests, X-ray imaging was performed on end-hooked fibres placed at angles of 0° and 30° to the loading direction. The embedment length ratio (length of fibre each side of the crack relative to the fibre length) was 0.5:0.5.

In the DS (Mode II) tests, gamma ray imaging was used with the fibres oriented at angles of 0° , $\pm 30^\circ$ and $\pm 60^\circ$ with respect to a plane perpendicular to the loading direction. Six tests were conducted, three with end-hooked fibres and three with straight fibres, with an embedment length ratio of 0.33:0.67. A further two tests were undertaken with end-hooked fibres at an embedment length ratio of 0.25:0.75. The details of the experimental program are outlined below.

2.2 Materials and fabrication of test specimens

Figure 1 shows the specimen dimensions and reinforcing arrangements for the Mode I fracture specimens and Figure 2 for the Mode II fracture specimens. The specimens were fabricated in two separate concrete pours. The fibre angle (θ) is measured from a horizontal line drawn normal to the interface of the two halves of the specimen. In the L-shaped shear specimens, a clockwise direction is considered as positive in the “2” configuration whereas an anticlockwise direction is negative. For example, the angle of orientation shown in Figure 2 is negative. The “2” or “2” configuration is taken as the reference or front face direction and the “5” or “5” configuration as the back face.

The thickness of the double L-shaped specimens was 40 mm. The L-shaped bars were 6 mm in diameter with a minimum cover of 5 mm and the yield strength of the bars was nominally 500 MPa. A single row of four fibres were cast into the matrix. The fibres were clamped into position for the first pour using timber packing clamps placed on the side of the specimen selected for the second pour. One day later, the timber clamps were released and the second side of the specimen was cast.

The tensile specimens were constructed in a similar manner to the shear specimens with two fibres were clamped into position on one side of the specimen while the mortar was cast on the other. The thickness of the specimens was 30 mm.

The mortar mix used in the specimens was composed of kiln dried Sydney sand and general purpose Portland cement mixed in a ratio of 3:1 (sand : cement) and water at a water : cement ratio of 0.4. No other additives used in the mix design.

The deformed steel fibres used in the tests were high strength, end-hooked Dramix cold drawn fibres produced by Bekaert (Belgium). The fibre dimensions and material properties are given in Table 1. The straight fibres used in the tests were made from end-hooked fibres with the hook portions cut-off.

Table 1. Properties of steel fibres.

Fibre type	Diameter, d (mm)	Length, l (mm)	Aspect ratio l/d	Tensile strength (MPa)
Hooked-ended	0.9	60	67	1085
Straight	0.9	48	53	1085

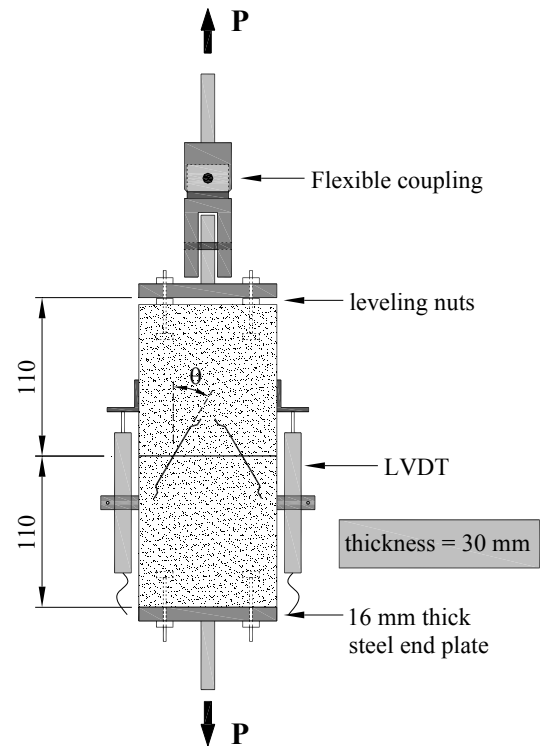


Figure 1. Testing arrangements for tensile specimen.

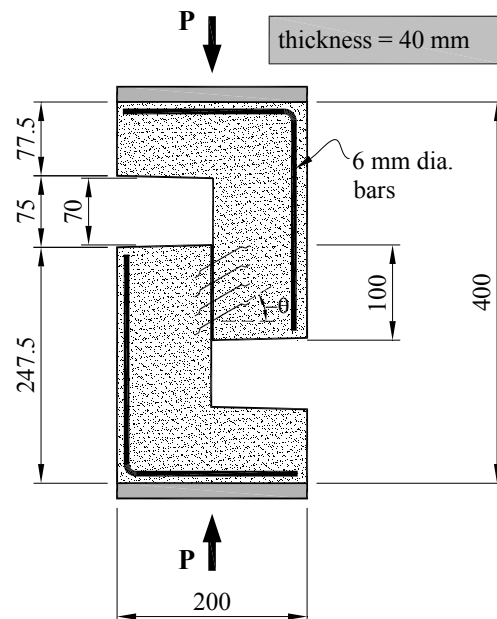


Figure 2. Push-off specimen dimensions and details.

Details of the test specimens for the radiographic imaging are given in Table 2. The specimens are designated as $NXXI\pm\theta Y a:b$ where N = “non-destructive test”, XX = DS for the “direct shear” and XX = UT for the “uniaxial tension” tests, $\pm\theta$ is the angle of the fibre taken from a line normal to the crack interface, Y is the fibre type (H = end-hooked fibres and S = straight fibres) and $a:b$ is the ratio of the fibre embedded on the short side to that of the long side. For example, specimen NDSI+60H1:3 is a non-destructive (radiographic imaging) test in direct shear with an end-hooked fibre at an angle of $+60^\circ$ and a fibre embedment length (l_e) of $l_e = 0.25l_f$ on the short side and $l_e = 0.75l_f$ on the long side (ie. short side embedment to long side embedment ratio is 1:3) where l_f is the total length of the fibre.

Table 2. Specimen properties.

Specimen	Test	Fibre Type	θ (deg.)	Cylinder Strength (MPa)
NDSI-60H1:3	Shear	hooked	-60	50
NDSI+0H1:3	Shear	hooked	0	50
NDSI+60H1:3	Shear	hooked	+60	50
NDSI-60S1:3	Shear	straight	-60	43
NDSI+0S1:3	Shear	straight	0	43
NDSI+60S1:3	Shear	straight	+60	43
NDSI-30H1:2	Shear	hooked	-30	32
NDSI+30H1:2	Shear	hooked	+30	32
NUTI±0H1:1	Tension	hooked	0	36
NUTI±30H1:1	Tension	hooked	30	36

The specimens were cast horizontally in two stages into the moulds. The first stage involved casting a section on one side of the cracking plane, with the other half of the specimen blocked out and the fibres protected between two timber sandwich blocks. The specimens were compacted on a vibrating table and then left to cure for 24 hours. After setting of the first half of the specimen, the timber blocks were removed from the second half of the specimen and the casting completed. The completed specimens were then air cured for 24 hours to allow setting then demoulded. Six 200 mm high by 100 mm diameter cylinders were cast for each half specimen for quality control.

After setting of the second half, the specimens and cylinders were stripped and placed in a water bath at 90°C for 3 days to accelerate the curing process. After removal from the hot water bath all the specimens were placed in a constant dry temperature room for 3 days to remove the excess water. Following the drying process all the specimens were removed from the dry temperature room and stored in a laboratory environment until testing. The mean cylinder compressive strength at the time of testing is given in Table 2.

2.3 Testing arrangements

The testing arrangements are shown in Figures 3 and 4 for the UT and DS tests, respectively. The displacements in the direction of movement of the loading jacks were measured using linear variable differential transducers (LVDTs). In the UT tests, two LVDTs were used, one placed on each side of the specimen and the displacement measurements were taken as the average of the LVDT readings. For the DS tests, one LVDT was used to measure the crack sliding displacements.

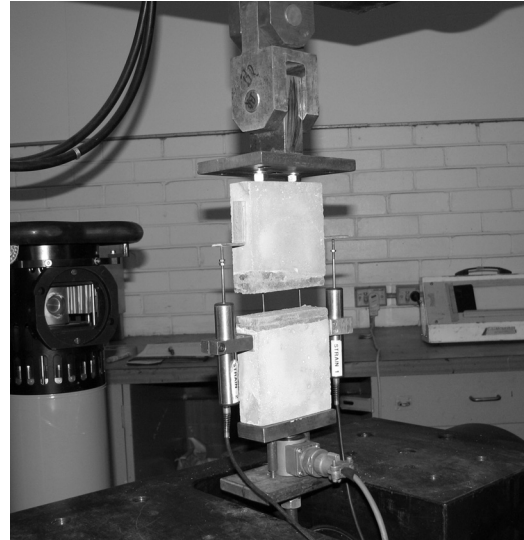


Figure 3. Testing arrangements for UT specimens.

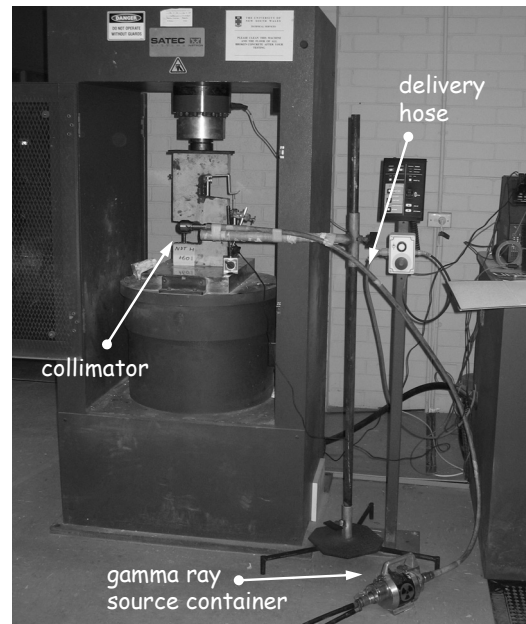


Figure 4. Testing arrangements for DS specimens.

3 TEST RESULTS

3.1 Introduction

The peak loads, displacements at the peak loads and failure mode are given in Table 3. The results of the radiographic imaging are presented in Sections 3.2 for the UT tests and 3.3 for the DS tests.

Table 3. Peak loads per fibre, displacements and failure modes.

Specimen	Average Peak load per fibre (N)	Slip at peak load (mm)	Failure mode
NDSI-60H1:3	390	28.6	FF
NDSI+0H1:3	680	3.3	PO
NDSI+60H1:3	460	0.6	PO
NDSI-60S1:3	230	16.9	FF/PO
NDSI+0S1:3	140	10.5	PO
NDSI+60S1:3	200	0.1	PO
NDSI-30H1:2	590	9.9	FF
NDSI+30H1:2	420	3.5	PO
NUTI±0H1:1	460	3.5	PO
NUTI±30H1:1	380	4.0	PO

Note: * FF = fibre fracture; PO = fibre pullout

3.2 Uniaxial Tension (UT) Tests

The UT tests were undertaken in an Instron universal testing machine under displacement control. The resulting load versus crack opening displacement (COD) diagrams are given in Figure 5 for the 0° fibre angle test and Figure 7 for the 30° angle fibre tests and the corresponding X-ray images are presented in Figures 6 and 8, respectively. The photo plate numbers are given as “Px” where x is the image number. The location of each X-ray image taken in the load-displacement space is indicated on the load-displacement figures.

The X-ray negative images were converted into positives using digital imaging and the fibres within the mortar matrix are untouched from those obtained from the X-ray photography. No image is obtained in the opened portion of the specimen (as the X-ray exposure time is set for the density and thickness of the specimen leaving the portion at the opening over exposed). In this region the fibres are interpolated based on visual observations.

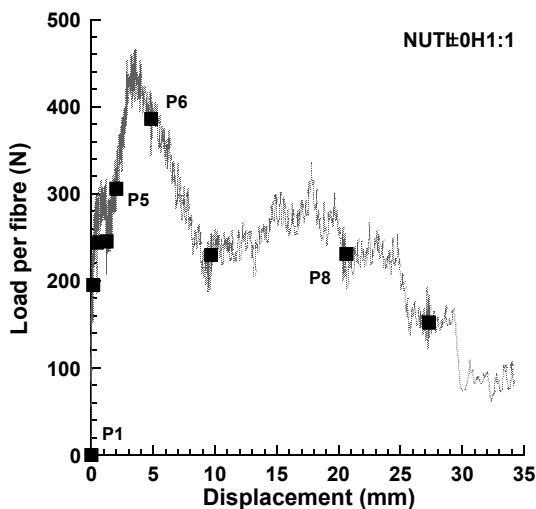


Figure 5. Load-displacement for specimen NUTI±0H1:1.

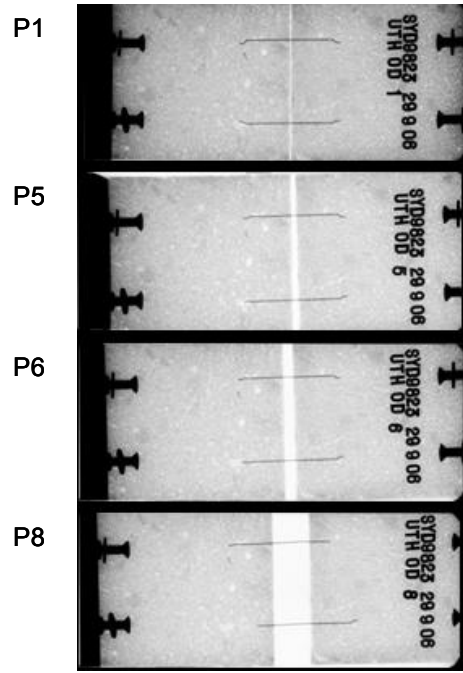


Figure 6. X-ray imaging for specimen NUTI±0H1:1.

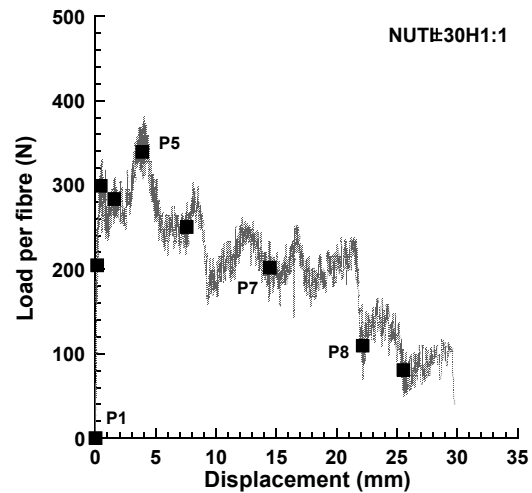


Figure 7. Load-displacement for specimen NUTI±30H1:1.

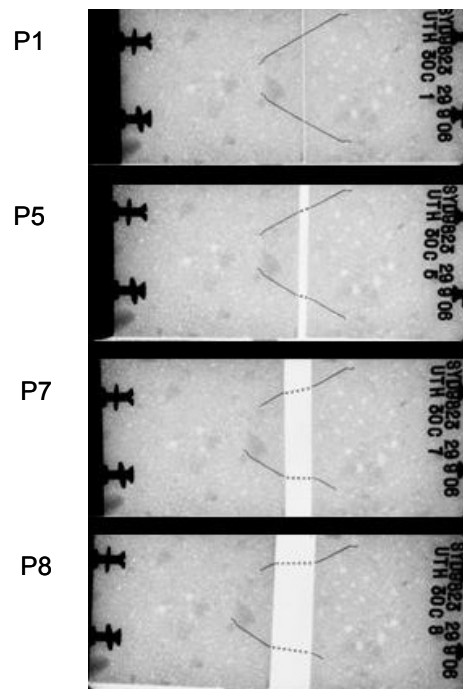


Figure 8. X-ray imaging for specimen NUTI±30H1:1.

3.3 Direct Shear (DS) Tests

The DS tests were conducted using a Satec testing machine under displacement control. Before testing, the weak bond on the shear plane of the mortar-mortar interface was broken and a layer of grease was applied along the 70 mm long vertical surfaces to reduce the effect of friction.

With the exception of the points of radiographic imaging, the displacement rate before the displacement corresponding to the peak load was 0.2 mm per minute. After peak, the rate was increased. Each specimen was loaded until full fracture had occurred.

As movement of the specimen blurs the radiographic image, the displacement rate was gradually reduced to zero before the film was exposed and held constant for the duration of the exposure. After the completion of the imaging the displacement rate was again set to that stated above.

In the DS tests, gamma rays were used for the radiographic imaging. For clear reproduction, the fibres images have been digitally enhanced. As for the UT tests, the fibre images within any gap in the specimen (due to horizontal displacements) are interpolated from visual observations.

Typical results for the end-hooked fibre specimens are given in Figures 9 to 14 with the location of the gamma ray imagery on the load-displacement histories, as indicated. Space precludes the presentation of the full sets of results in this paper and the reader is referred to the laboratory testing report by Lee and Foster (2006c) for the complete test results.

As for the tests of Lee and Foster (2006a, 2006b), it was observed that a number of fibres pulled out from the longer embedded side. For example, see the lower fibre of specimen NSDI+0H1:3 in Figure 14. Despite the bias by a factor of 3 in favour of the short side it is clearly observed that the fibre pulled out from the longer embedded side. The reasons for this behaviour are discussed further in Section 4 of this paper.

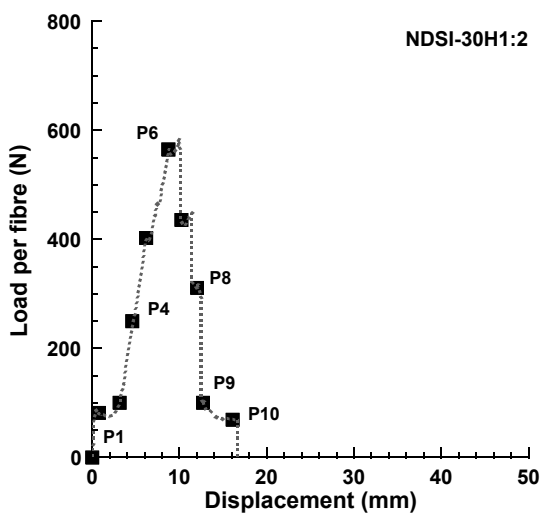


Figure 9. Load-displacement for specimen NDSI+30H1:2.

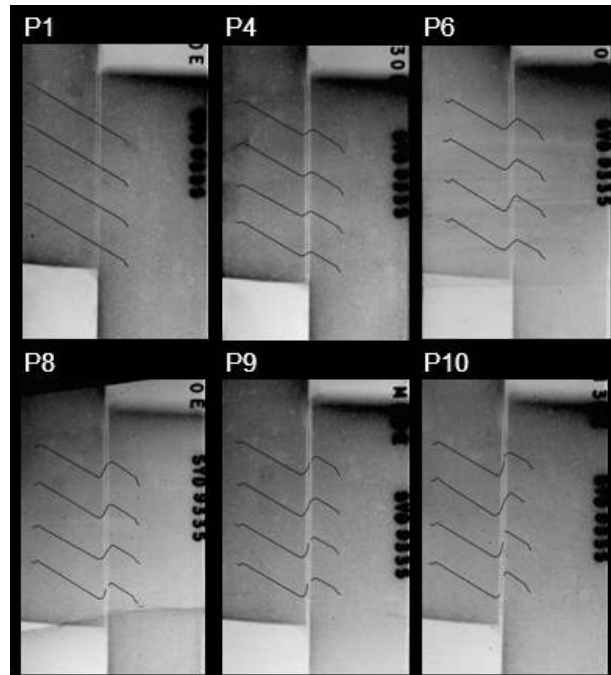


Figure 10. Gamma ray imaging for specimen NDSI-30H1:2.

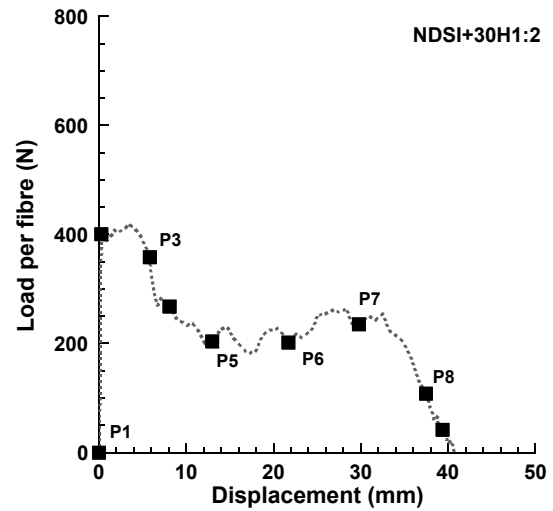


Figure 11. Load-displacement for specimen NDSI+30H1:2.

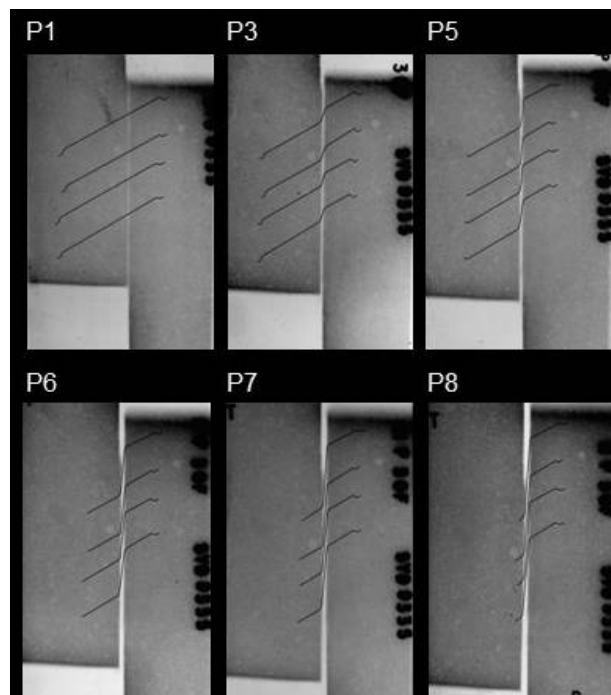


Figure 12. Gamma ray imaging for specimen NDSI+30H1:2.

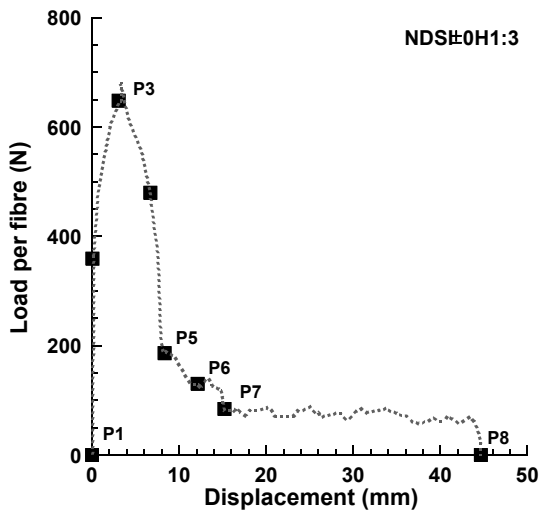


Figure 13. Load-displacement for specimen NDSI±0H1:3.

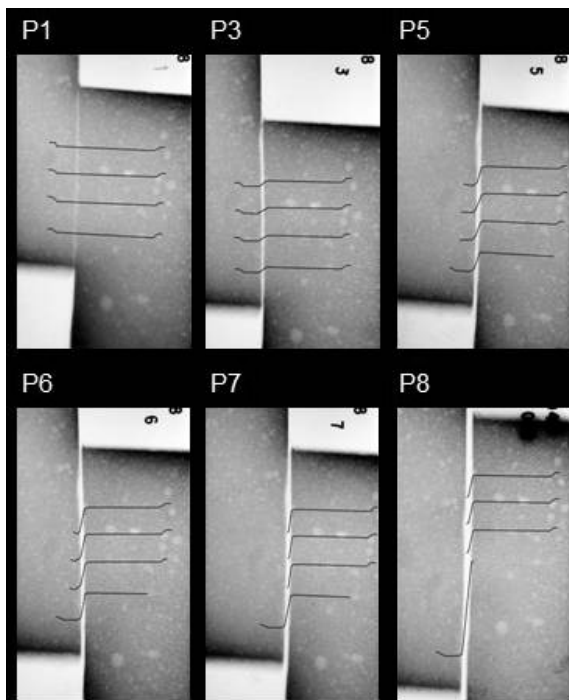


Figure 14. Gamma ray imaging for specimen NDSI±0H1:3.

In this study together with that of Lee and Foster (2006a) a total of 47 tests were conducted on DS specimens with 4, 6 or 8 fibres per specimen. In total, observations on 434 fibres were recorded. A survey of the results is presented in Table 4 showing the mode of failure for each fibre and, where failure was by pullout (PO), which side the fibre pulled out from (left or right for the equal embedment length specimens; short or long for the unequal embedment length specimens).

Table 4. Survey of discrete fibre failures.

Specimen Group	Fracture	Total PO	PO _{Left}	PO _{Right}	PO _{Long}	PO _{Short}
DSI±0H1:1	26	58	23	35	-	-
DSI±0H1:3	27	51	-	-	8	43
DSI±0S1:1	7	65	36	29	-	-
DSI±0S1:3	12	60	-	-	33	27
NDSI±0H1:3	33	31	-	-	7	24
NDSI±0S1:3	14	30	-	-	1	29
NDSI±0H1:2	8	12	-	-	7	5

4 ANALYSIS OF RESULTS

The fibre reinforced specimens failed in one of three modes: fibre pullout, fibre fracture or in a mixed mode with some fibres in the specimen pulling out from the matrix while others fractured.

For straight fibres, the initial stage for fibre pullout is an elastic response which is typically linear. In this stage the fibres remain fully bonded to the surrounding matrix. The next stage is partial debonding followed by slippage or frictional pullout until the fibre is completely pulled through the fibre tunnel where the fibre tunnel is the space that was previously occupied by the fibre. If end appendages such as hooks are present, then a mechanical clamping stage is introduced before significant slippage takes place (Alwan et al. 1999).

The initial elastic response for the hooked-ended and straight fibres with positive angles of orientation was reasonably linear. However, for the shear tests, as the angle became increasingly more negative, considerable vertical displacement occurred prior to the mechanical engagement of the fibre. A similar observation was made by Voo and Foster (2003, 2004) for fibres subjected to uniaxial tension but this effect is exaggerated in the case of the fibres subjected to crack sliding. The effect of the local damage to the fibre and the increased snubbing effect for crack sliding are shown clearly when comparing the images in Figures 10 and 12 for the DS tests compared to the 30° UT specimen shown in Figure 8. In fact, the effect of snubbing is shown to dominate the failure of the zero and negative angled fibre specimens.

Examining closely the images of specimen NDSI-30H1:2 in Figure 10, it is seen that the effect of increased bond of the fibres due to snubbing cause the fibres to fracture. In P6 the specimen is observed to be carrying a load of 590 N with all fibres intact. Shortly afterwards, however, it is seen that the bottom fibre has fractured (P8) and in P10 three of the four fibres have fractured. Because of the fibre fractures, the load versus displacement graph (Figure 9) shows the specimen to have a somewhat brittle response. On the other hand, NDSI+30H1:2 is more ductile albeit with a lower peak load of 420 N. In this case all fibres pullout from the specimen.

In Figure 15 the peak loads are plotted (on the left axis) against the fibre angle for the end hooked (EH) specimens reported here and in Lee and Foster (2006a, 2006b). It is seen that in the EH tests that fibres angled as high as +75° have a significant capacity. The strength increases, with the increased anchorage due to snubbing, until the point where the anchorage is sufficiently high to cause fracture of the fibres. In the tests undertaken in this study, this is at approximately -30°.

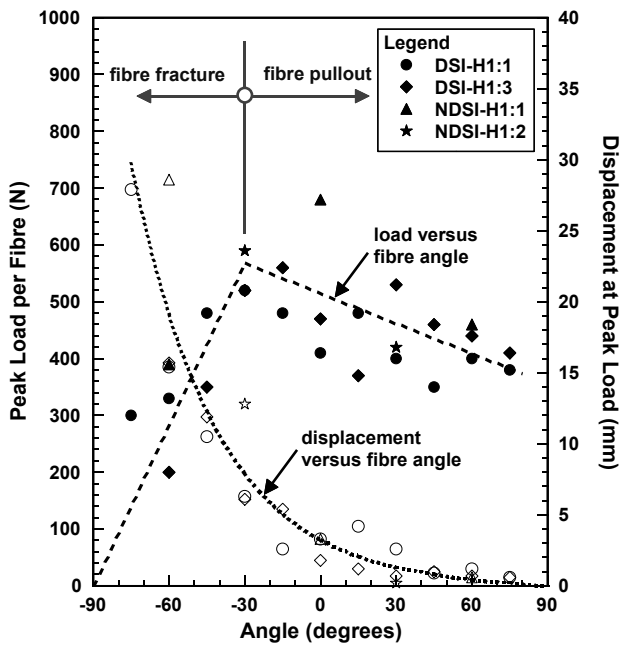


Figure 15. Hooked-end fibre tests: peak load and displacement at peak load versus fibre angle (solid data markers peak load versus fibre angle; hollow data markers displacement at peak load versus fibre angle).

A second point of interest is that the relative length of embedment each side of the crack interface appears to have little influence on the peak load. This is because the greater part of the fibre force is developed at the hook and in the snubbing zone and the straight portion of fibre between these points has a significantly smaller influence on the failure load. Note that the difference between the shorter and longer embedded parts of the fibre is the length of this straight portion. Variations in bond in the snubbing zone is sufficient to ensure a number of fibres pullout from the longer embedded side even for specimens with embedment ratios as high as 1:3.

The effect of the high anchorage in the snubbing zone on each side of the crack plane is evidenced by the large number of fibres that were observed to pull out from the longer embedded side. For example, for the DSI±0H1:3 and NDSI±0H1:3 series of tests, of the 82 fibres that pulled out from the specimens, 15 pulled out from the longer embedded side. For the DSI±0S1:3 and NDSI±0S1:3 tests, 34 of 90 fibre pullout failures were from the longer embedded side. The effect of this is that the tail of the curve extends to a displacement approximately equal to the longer embedment length. For example, in specimen NDSI+0H1:3 (Figure 13) P5 and P6 show that three of the four fibres pulled out from the short side. By P7 (15.2 mm displacement) these fibres had completely pulled out from the matrix. Complete fracture did not occur, however, until 44.6 mm displacement (P8) when the fourth fibre pulled out from the long side.

While in Figure 15 it is seen that fibres orientated at angles between -30° and $+75^{\circ}$ sustain a significant load, as the fibre angle decreases the displacement

corresponding to this peak load increases significantly. Thus, in a fibre composite only those fibres at high positive angles are likely to be effective in carrying load over the engineering range of a few millimetres. That is, half or more of the fibres do not carry load efficiently. For the straight fibre tests (Figure 16) the fibres at the high positive angles do not carry significant load and those at lower angles do not engage until significant movement has occurred and are prone to fracture.

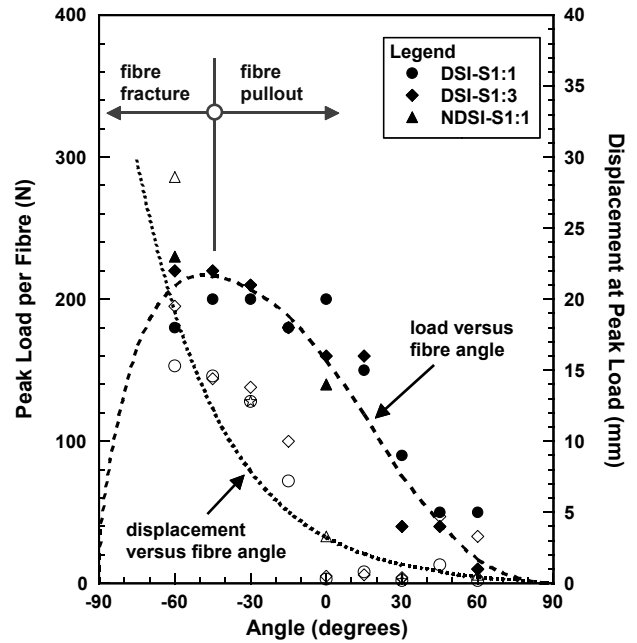


Figure 16. Straight fibre tests: peak load and displacement at peak load versus fibre angle (solid data markers peak load versus fibre angle; hollow data markers displacement at peak load versus fibre angle).

Comparing Figures 15 and 16 it is demonstrated that straight fibres are inefficient in carrying longitudinal shear forces where concrete blocks are separated by smooth surfaces. Such might be the case, for example, in reactive powder concrete where large aggregate particles are eliminated from the mix. Further research is needed, however, for conventional concrete where sliding maybe combined with crack opening and tension across a crack face forced by aggregate particles sliding over one another.

The survey data in Table 4 can be used to determine the probability that a fibre pulls out from the longer embedded side. In the development of material models for design this observation needs consideration. For the data set that includes only pullout failures, a probability function is developed representing the statistical likelihood that any discrete fibre will pullout from the longer embedded side. The boundary conditions for such a function are: (i) for a fibre with a short to long side embedment ratio of 0:1, the probability of failure from the longer embedded side is zero; (ii) for a fibre with a short to long side embedment ratio of 1:1, the probability of

failure from the shorter embedded side is 0.5; (iii) for a fibre with a short to long side embedment ratio of 0:1, the slope of the probability function is zero; and (iv) for a fibre with a short to long side embedment ratio of 1:1, the slope of the probability function approaches zero. A simple function that meets the boundary conditions is

$$\gamma_l = 0.5 \left(1 - e^{-a\lambda^3} \right) \quad (1)$$

where γ_l is the probability that an individual fibre will pullout from the longer embedded side, λ is the ratio of shorter to longer fibre embedment lengths ($l_{e,short} / l_{e,long}$) and a is a fitting constant. The resulting function is shown in Figure 17 with $a = 12.3$ and $a = 38.1$ for the EH and straight fibres, respectively.

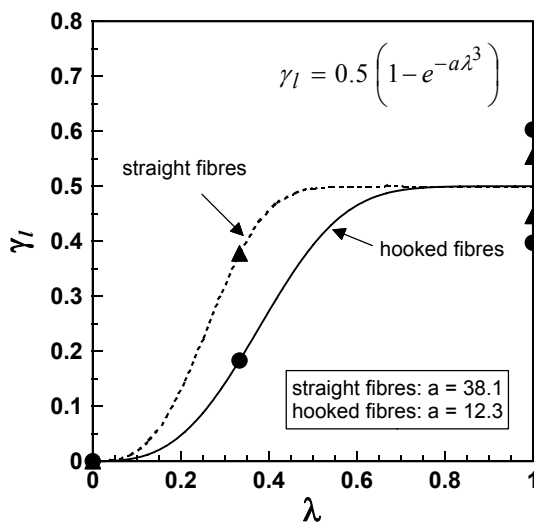


Figure 17. Probability that a fibre will pullout from the longer embedded side.

5 CONCLUSIONS

Radiographic imaging has proved to be a valuable tool in understanding the behaviour of discrete fibres in a cementitious matrix. Two types of radiographic imaging were used: gamma ray and X-ray. Of the two methods, the more powerful X-rays proved superior with the fibres being clearly identified at all stages of testing.

The imaging has shown the importance of the snubbing effect on the behaviour of fibre reinforced mortar subjected to Mode II fracture. In particular, it is shown that fibres subjected to shear across a crack face behave very differently to that of crack opening. The snubbing effect dominates the behaviour and the angle of a fibre crossing a crack is an important parameter in determining behaviour and failure mode.

Lastly, it has been shown that there is a statistical chance that fibres pullout from the longer embedded side and a probability function is proposed to predict the likelihood of this event.

ACKNOWLEDGMENTS

This study is funded via Australian Research Council (ARC) discovery grant DP0559742. The support of the ARC is acknowledged with thanks.

REFERENCES

- Alwan, J.M., Naaman, A.E. & Guerrero, P. 1999. Effect of mechanical clamping on the pull-out response of hooked steel fibers embedded in cementitious matrices. *Concrete Science and Engineering*, 1(3): 15-25.
- Balaguru, P. & Dipsia, M.G. 1993. Properties of fiber reinforced high-strength semilightweight concrete. *ACI Materials Journal*, 90(5): 399-405.
- Banthia, N. & Trottier, J.F. 1994., Concrete reinforced with deformed steel fibres, part 1: bond-slip mechanisms, *ACI Materials Journal*, 91(5): 435-446.
- Khaloo, A.R. & Kim, N. 1997. Influence of concrete and fiber characteristics on behaviour of steel fibre reinforced concrete under direct shear. *ACI Materials Journal*, 94(6): 592-601.
- Lee, G.G. & Foster, S.J. 2006a. Behaviour of steel fibre reinforced mortar in shear I: Direct shear tests. *UNICIV Report No R-444, The University of New South Wales, Sydney*: 1-185.
- Lee G.G. & Foster, S.J. 2006b. Direct shear tests with gamma ray imaging on steel fibres in cementitious materials, *Proceedings, 19th Australasian Conference on the Mechanics of Structures and Materials*, ACMSM 19, Nov 29 - Dec 1, Christchurch, New Zealand.
- Lee, G.G. & Foster, S.J. 2006c. Behaviour of steel fibre reinforced mortar in shear II: Gamma ray imaging. *UNICIV Report No R-445, The University of New South Wales, Sydney*: 1-89.
- Mirsayah, A.A. & Banthia, N. 2002. Shear strength of steel fiber-reinforced concrete. *ACI Materials Journal*, 99(5): 473-479.
- Peterson, S.R., 1980. Fracture mechanical calculations and tests for fibre-reinforced cementitious materials. *Proceedings, Advanced in Cement Matrix Composites*, Mat. Res. Soc., Annual Meeting, Boston: 95-106.
- Romualdi, J.P. & Batson, G.B. 1963. Behaviour of Reinforced Concrete Beams with Closely Spaced Reinforcement. *Journal of the American Concrete Institute*, 60(6): 775-790.
- Valle, M. & Büyüköztürk, O. 1993. Behaviour of fiber reinforced high strength concrete under direct shear. *ACI Materials Journal*, 90(2): 122-133.
- Van de Loock, L. 1987. Influence of steel fibres on the shear transfer in cracks. *Proceedings of the international symposium on fibre reinforced concrete, Madras, India, 16-19 December*. Rotterdam: Balkema.
- Voo, J.Y.L. & Foster, S.J. 2003. Variable engagement model for fibre reinforced concrete in tension', UNICIV Report R-420, School of Civil and Environmental Engineering, The University of New South Wales, Australia: 86pp.
- Voo, J.Y.L. & Foster, S.J. 2004. Tensile fracture of fibre reinforced concrete: Variable engagement model. *Sixth Rilem symposium on fibre reinforced concrete (FRC), Varenna, Italy, 20-22 September*. Bagnaux: RILEM.